ONLINE MATERIALS (APPENDIX 1, FIGURES AND TABLES) FOR: A COMPARATIVE STUDY OF TWO PHASE EQUILIBRIA MODELING TOOLS: MORB EQUILIBRIUM STATES AT VARIABLE PRESSURE AND H_2O CONCENTRATIONS

Hernández-Uribe et al.

As noted in the "*Petrological modeling*"section, all calculations in this study are computed as equilibrium state points. Thus, we emphasize that although the Figures 1, 2, 4–7, and Supplementary Figures S1–S2 proceed up temperature from near-soliuds toward near-liquidus (i.e., equilibrium partial melting), the calculations are equally applicable to down-temperature equilibrium crystallization since there is no fractionation of solids from liquid.

EQUILIBRIUM STATES OF N-MORB AT 0.25 GPa

Phase relations

Low-H_2O. Phase relations calculated with rhyolite-MELTS are shown in Figures 1a and S1a. At temperatures near the liquidus, rhyolite-MELTS predicts clinopyroxene at ~1200 °C followed by plagioclase at 1190°C and orthopyroxene at ~1050 °C. Plagioclase and orthopyroxene proportions increase as temperature decreases until ~830 °C. Clinopyroxene proportion increases until orthopyroxene stabilizes and then decreases its proportion. Minor phases include magnetite and ilmenite; magnetite is stable from ~1110 °C to the end of the calculated path at low temperatures, whereas ilmenite is stable in the temperature interval ~980–940 °C. The proportion of solids is higher than the liquid fraction below ~1130 °C. The system becomes H_2O-saturated at ~880–870 °C.

Phase relations for HPx-mb16 are shown in Figure 1c and S1c. HPx-mb16 predicts clinopyroxene and plagioclase at temperatures above the liquidus calculated by rhyolite-MELTS (i.e., >1200 °C). Orthopyroxene stabilizes at ~1060 °C and amphibole joins the assemblage at ~930 °C. Plagioclase, orthopyroxene, and amphibole increase their proportion as temperature decreases; on the other hand, clinopyroxene proportions increase until amphibole stabilizes. Minor phases include olivine, titanite, rutile, and ilmenite. Olivine is stable within the temperature range ~970–930 °C. Titanite is stable within ~1250—1160 °C, whereas rutile is stable within ~1180–1060 °C and ilmenite from ~1090 °C to the end of the calculated path. The proportion of solids is higher than the

proportion of liquid below ~1090 °C. Fluid is never in excess at any given P–T conditions as temperature decreases.

High-H_2O. Phase relations calculated with rhyolite-MELTS are shown in Figure 1b and S1b. rhyolite-MELTS predicts olivine stabilization at ~1150 °C and clinopyroxene at ~1110 °C. Orthopyroxene stabilizes at the expense of olivine at ~970 °C. Plagioclase joins the assemblage at ~950 °C. Olivine proportions increase until orthopyroxene stabilizes and olivine is consumed. Plagioclase proportion increases until 830 °C, the end of the calculated conditions at low temperatures. Clinopyroxene increases its proportion considerably until plagioclase joins the assemblage. The single minor phase is magnetite, which is stable below ~1020 °C. The proportion of solids is higher than the proportion of liquid below~950 °C. The system becomes fluid-saturated at ~990 °C.

Phase relations for HPx-mb16 are shown in Figure 1d and S1d. At temperatures near the liquidus, HPx-mb16 predicts clinopyroxene at temperatures above the liquidus calculated by rhyolite-MELTS (i.e., >1100 °C). Plagioclase follows clinopyroxene and stabilizes at ~1080 °C. Amphibole joins the phase assemblage at ~980 °C. Orthopyroxene is stable within ~970–850 °C. Plagioclase and amphibole increase their proportions as temperature decreases. By contrast, clinopyroxene proportions increases until amphibole stabilizes. Minor phases include olivine, titanite, rutile, and ilmenite. Olivine is stable between ~970–930 °C. Titanite is stable within ~1200–1080 °C, whereas rutile is stable within ~1090–1050 °C and ilmenite below ~1070 °C. The proportion of solids is higher than the liquid proportion below ~980 °C. The system becomes fluid-saturated at ~1100 °C.

Liquid compositions

Low-H_2O. Liquid compositions evolve from basaltic near the liquidus to trachytic closer to the solidus (SiO_2 ranging from 50 to 56 wt% and Na_2O + K_2O from 3 to 9 wt%; Figs. 3a, 4a and d; Table S2) in both models. Compositions predicted by rhyolite-MELTS are SiO_2-poor but Al_2O_3-, FeO^t + MgO-, and CaO-rich close to the liquidus and evolve to SiO_2- and alkali-rich compositions near the solidus; at lower temperatures, liquids are more hydrous (Fig. 4; Table S2). Clinopyroxene stabilization promotes a slight increase in Al_2O_3 and FeO^t + MgO and a decrease in CaO as the liquid stabilizes (Figs. 4b, c, and e). When plagioclase and magnetite join the assemblage, Al_2O_3- and FeO^t + MgO begin to

decrease in the liquid down temperature, respectively (Figs. 4b and c). The last liquid fractions are Al_2O_3-richer and H_2O-poorer when H_2O is in excess (Figs. 4b and f).

Calculated HPx-mb16 liquid compositions are relatively SiO_2-poor and CaO-rich close the liquidus and evolve to relatively more hydrous and silica and alkali-rich compositions at lower temperatures (Fig. 4; Table S2). The Al_2O_3 and FeO^t + MgO contents show a relatively complex evolution; in general, close to the liquidus, liquids are enriched in these components compared to low-T liquids (Figs. 4b and c; Table S2). Ilmenite and olivine stabilization promote depletion in FeO^t + MgO in the liquid, and the latter further promotes an increase in the liquid's Al_2O_3 content down temperature (Figs. 4b and c).

High-H_2O. Liquid compositions evolve from basaltic near the liquidus to trachytic (in rhyolite-MELTS) and dacitic (in HPx-mb16) closer to the solidus (SiO_2 ranging from 49 to 67 wt% and Na_2O + K_2O from 3 to 9 wt%; Figs. 3b, 5a and d; Table S2). Liquid compositions calculated with rhyolite-MELTS are relatively SiO_2-poor, and FeO^t + MgO- and CaO-rich close to the liquidus and evolve to relatively silica- and alkali-rich compositions at lower temperatures; low-T liquids are also more hydrous than at higher temperatures (Fig. 5; Table S2). Clinopyroxene stabilization promotes a slight increase in Al_2O_3 and decrease in CaO in the liquid down temperature (Figs. 5b and e). When plagioclase stabilizes, liquid composition gets depleted in Al_2O_3 (Fig. 5b).

The calculated HPx-mb16 liquid compositions are relatively SiO_2-poor, and FeO^t + MgO- and CaO-rich at higher temperatures and evolve to compositions enriched in SiO_2-, alkali, and H_2O contents (Fig. 5; Table S2). High-T liquids are enriched in Al_2O_3 compared to the low-T liquids (Fig. 5b; Table S2). Olivine and orthopyroxene stabilization at high temperatures promote depletion in FeO^t + MgO in the liquid (Fig. 5c). When plagioclase joins the mineral assemblage, the liquid evolves to Al_2O_3- and CaO-poorer compositions down temperature (Figs. 5b and e). Under H_2O-saturated conditions, the liquid's H_2O content stabilizes but increases again when amphibole stabilizes (Fig. 5f).

EQUILIBRIUM STATES OF N-MORB AT 1 GPa

Phase relations

Low-H_2O. Phase relations calculated with rhyolite-MELTS are shown in Figure 2a and S2a. Rhyolite-MELTS predicts clinopyroxene at ~1320 °C followed by plagioclase at

~1200 °C; garnet joins the mineral assemblage at ~1190 °C. Plagioclase and garnet proportions increase as temperature decreases until 760 °C, the end of the calculations. Clinopyroxene proportion increases until garnet stabilizes and then slightly decreases. Minor phases include quartz, analcime, and biotite; quartz is stable below 910 °C, whereas analcime and biotite are stable below ~780 °C and ~770 °C, respectively. The proportion of solids is higher than the proportion of liquid below ~1130 °C. The system is never H_2O-saturated.

Phase relations for HPx-mb16 are shown in Figure 2c and S2c. HPx-mb16 predicts clinopyroxene at temperatures above the liquidus calculated by rhyolite-MELTS (i.e., >1320 °C; Fig. 2c). Plagioclase stabilizes at ~1270 °C followed by orthopyroxene at ~1110 °C which is later consumed at ~880 °C. Amphibole joins the assemblage at ~1040 °C whereas garnet stabilizes at ~980 °C. Clinopyroxene and plagioclase proportions increase as temperature decreases until amphibole and garnet crystallize, respectively; afterwards, their proportions slightly decrease. By contrast, garnet and amphibole proportions increase until the end of the run at low temperatures. Minor phases include quartz, titanite, rutile, and ilmenite. Quartz is stable below ~900 °C. Titanite is stable within ~1350–1270 °C, whereas rutile is stable within ~1300–1060 °C and ilmenite between~1080–1070 °C. After ilmenite is consumed, rutile reappears and is stable until the end of the run. The proportion of solids is higher than the liquid proportion below ~1150 °C. Fluid is never in excess at any given temperature as temperature decreases.

High-H_2O. Phase relations calcualted with rhyolite-MELTS are shown in Figure 2b and S2b. Rhyolite-MELTS predicts clinopyroxene stabilization at ~1200 °C followed by garnet at ~1130 °C. Analcime is stable at ~840 °C whereas amphibole joins the assemblage at ~710 °C. Clinopyroxene proportion increases until amphibole stabilizes, which increases its proportion at expense of clinopyroxene. Garnet proportion increases until analcime joins the assemblage, and after that point, garnet proportion remains relatively constant. Analcime and amphibole proportions increase until 600 °C, the end of the calculated conditions at low temperatures. Minor phases include orthopyroxene, quartz, biotite, and muscovite; orthopyroxene is stable only within ~1150–1120 °C and quartz below ~750 °C. Biotite is stable at ~660 °C until muscovite joins the assemblage at 610 °C and consumes biotite. The proportion of solids is higher than the proportion of liquid below ~1070 °C. The system becomes H_2O-saturated at ~630 °C.

Phase relations for HPx-mb16 are shown in Figure 2d and S2d. HPx-mb16 predicts clinopyroxene at temperatures above the liquidus calculated by rhyolite-MELTS (i.e., >1200 °C). Amphibole stabilizes at ~1080 °C followed by quartz at ~800 °C. Clinopyroxene proportion increases as temperature decreases until amphibole stabilizes, after which its proportion decreases. By contrast, amphibole and quartz proportions increase until the end of the run. Minor phases include garnet, epidote, plagioclase, titanite, and rutile. Garnet is stable within ~910–810 °C, and epidote and plagioclase below ~730 °C and ~650 °C, respectively. Titanite is stable within ~1250–1200 °C, and then stabilizes again at ~860 °C. Rutile is stable within ~1250–980 °C and ilmenite between ~1080–1070 °C. The proportion of solids is higher than the liquid fraction below ~980 °C. The system becomes H_2O-saturated at ~700 °C.

Liquid compositions

Low-H_2O. Liquid compositions evolve from basaltic near the liquidus to trachytic (in rhyolite-MELTS) and dacitic (in HPx-mb16) closer to the solidus (SiO_2 ranging from 51 to 74 wt% and Na_2O + K_2O from 3 to 8 wt%; Figs. 3c, 6a and d; Table S3). Calculated compositions with rhyolite-MELTS are, in general, relatively SiO_2-poor but Al_2O_3-, FeO^t + MgO-, and CaO-rich at higher temperatures and evolve to SiO_2-, alkali-, and H_2O-rich compositions near the solidus (Fig. 6; Table S3). Clinopyroxene stabilization promotes a slight increase in Al_2O_3 and decrease in CaO in the liquid down temperature (Figs. 6b and e). When plagioclase joins the assemblage, liquid evolves to Al_2O_3-poorer compositions (Fig. 6b). Quartz stabilization promotes alkali-enrichment and SiO_2-depletion in the liquid (Fig. 6a). The stabilization of biotite further promotes Al_2O_3-enrichment and H_2O-depletion in the calculated composition (Figs. 6b and f).

Liquid compositions calculated using HPx-mb16 are SiO_2-poor and Al_2O_3-, FeO^t + MgO-, and CaO-rich close the liquidus and evolve to compositions enriched in SiO_2, alkalis and H_2O (Fig. 6; Table S3). The Al_2O_3 and FeO^t + MgO contents show a relatively complex evolution. When plagioclase joins the mineral assemblage at high temperatures, the liquid evolves to FeO^t + MgO-richer and Al_2O_3- and CaO-poorer compositions (Figs. 6b, c, and e). Subsequent ilmenite and amphibole stabilization promotes depletion in FeO^t + MgO and enrichment in Al_2O_3 in the liquid (Figs. 6b and c).

High-H_2O. Liquid compositions evolve from basaltic near the liquidus to tephrite-basanitic (in rhyolite-MELTS) or trachytic (in HPx-mb16). Liquid compositions in rhyolite-MELTS are, in general, Al_2O_3-, FeO^t + MgO-, and CaO-rich close to the liquidus and evolve to alkali- and H_2O-rich compositions near the solidus (Fig. 7; Table S3). The SiO_2-content evolution is relatively more complex; liquid fractions closer to the liquidus are SiO_2-poor but increase as temperature decreases; when quartz joins the assemblage, the liquid gets significantly depleted in SiO_2 (Fig. 7a). Clinopyroxene stabilization promotes a slight increase in Al_2O_3 and decrease in CaO in the liquid down temperature (Figs. 7b and e). When garnet joins the assemblage, liquid evolves towards Al_2O_3-depleted compositions (Fig. 7b). Analcime and quartz stabilization promote alkali-depletion and -enrichment, respectively (Fig. 7d). The latter phase further promotes H_2O-enrichment in the liquid (Fig. 7f).

HPx-mb16 liquid compositions are SiO_2-poor and Al_2O_3-, FeO^t + MgO-, and CaO-rich close the liquidus and evolve to compositions enriched in SiO_2, alkalis, and H_2O (Fig. 7; Table S3). High-T liquids are SiO_2-poor but evolve to SiO_2-rich compositions as temperature decreases until quartz joins the assemblage, after which the liquid evolves to SiO_2-poorer compositions (Fig. 7a). Significant amphibole stabilization promotes depletion in FeO^t + MgO and enrichment in Al_2O_3 in the liquid down temperature (Figs. 7b and c).

MINERAL COMPOSITIONS

For this study, clinopyroxene, plagioclase, orthopyroxene, and garnet calculated compositions were compared between different thermodynamic models. In some runs, rhyolite-MELTS predicts two stable clinopyroxene at a given P–T condition; below, we only describe the composition of the most abundant clinopyroxene. Compositional evolution of these phases is shown in the Figures S3–S6. When more than one clinopyroxene is stable at a given P–T point in rhyolite-MELTS, their masses were summed together. Because amphibole stability is limited in rhyolite-MELTS calculations, amphibole composition comparison was made in the temperature range of 700–600 °C every 20 °C (Table S4).

Equilibrium states of N-MORB at 0.25 GPa

Clinopyroxene. Mineral compositions are shown in Figure S3. In general, clinopyroxene predicted by both modeling setups is augitic to diopsidic regardless of the bulk H_2O

content. Clinopyroxene compositions calculated with rhyolite-MELTS are relatively Si-, Mg#-, and X_{Fe3+}-rich at higher temperatures and decrease with decreasing temperature as Al increases. In the low-H_2O run, clinopyroxene Ca content decreases and Fe^{2+} content increases with decreasing temperature until orthopyroxene joins the mineral assemblage; after that temperature, the Ca content increases and the Fe^{2+} content does not change with decreasing temperature. On the other hand, in the high-H_2O run, the Ca and Fe^{2+} content slightly increase with decreasing temperature. Here, orthopyroxene stabilization does not affect the clinopyroxene composition.

HPx-mb16 clinopyroxene is relatively Al-, Mg#-, and X_{Fe3+}-rich at higher temperatures. In contrast to rhyolite-MELTS, clinopyroxene Si and Fe^{2+} increase with decreasing temperature. Clinopyroxene Ca content decreases with decreasing temperature until orthopyroxene joins the mineral assemblage; after that temperature, the clinopyroxene's Ca slightly increases.

Plagioclase. Mineral compositions are shown in Figure S4. Plagioclase anorthite content decreases with decreasing temperature in both models; in both low- and high-H_2O runs, plagioclase is always richer in anorthite content. Rhyolite-MELTS predicts albite-rich compositions at < 880 °C.

Orthopyroxene. Mineral compositions are shown in Figure S5. Modeled orthopyroxene compositions are similar regardless of the model and follow the same compositional trends with decreasing temperature. All orthopyroxene compositions correspond to enstatite. Orthopyroxene Si content increase as temperature decreases but the Al and Ca contents and the Mg# and X_{Fe3+} decrease with decreasing temperature.

Equilibrium states of N-MORB at 1 GPa

Clinopyroxene. Mineral compositions are shown in Figure S3. Calculated clinopyroxene compositions are augitic to diopsidic in both models. In the low-H_2O rhyolite-MELTS run, clinopyroxene's Si and X_{Fe3+} decrease with decreasing temperature as Al increases. Clinopyroxene Mg# and Ca contents decrease until garnet stabilizes; the Fe^{2+} content follows the opposite trend. In the high-H_2O runs, the Si, X_{Fe3+}, and Al follow the same trends; the Ca content and Mg# increase with decreasing temperature, whereas the Fe^{2+} content decreases with decreasing temperature. Amphibole and muscovite stabilization

promote decrease in Al and an increase in Si. The Ca content increases when garnet joins the mineral assemblage.

In the HPx-mb16 calculations, clinopyroxene Al, Mg#, and X_{Fe3+} decrease as temperatures decreases but Si and Fe^{2+} increase in both the low- and high-H_2O runs. In the low-H_2O run, the clinopyroxene Ca content decreases until orthopyroxene joins the assemblage. By contrast, the clinopyroxene Ca content in the high-H_2O run increases with decreasing temperature until epidote joins the assemblage.

Plagioclase. Mineral compositions are shown in Figure S4. Plagioclase anorthite content decrease with decreasing temperature regardless of the model; in the high-P–low-H_2O run, plagioclase is always richer in anorthite content. Rhyolite-MELTS predicts albite-rich compositions at < 1160 °C and HPx-mb16 at < 900 °C.

Amphibole. In rhyolite-MELTS, amphibole is only stable in the high-H_2O run whereas HPx-mb16 predicts amphibole. All calculated amphibole compositions in rhyolite-MELTS correspond to actinolite. Amphibole Si pfu content remains without change when temperature decreases, whereas the Ca contents increase and the Mg# slightly decreases with decreasing temperature (Table S4). In comparison, amphiboles in HPx-mb16 correspond to pargasite. Amphibole Si pfu content increases and Al content decreases as temperature decreases but Na and the Mg# increase whereas Ca decreases with decreasing temperature (Table S4).

Garnet. Mineral compositions are shown in Figure S6. Garnet compositions are almandine-rich; almandine and grossular contents increase with decreasing temperature whereas the pyrope content decreases.

Comparison of the calculated mineral compositions

Clinopyroxene compositions are similar in all runs in that the overall compositions predicted correspond to augitic-diopsitic compositions. However, clinopyroxene Si contents are slightly lower (although similar at higher temperatures) whereas Al and X_{Fe3+} are slightly higher in rhyolite-MELTS compared toHPx-mb16 calculations at any given temperature. The Mg# is relatively similar, with the exception of the high-P–low- and high-H_2O runs, where the Mg# is higher in rhyolite-MELTS at lower temperatures.

Clinopyroxene Fe^{2+} contents are systematically higher in HPx-mb16 at lower temperatures but relatively similar or higher in rhyolite-MELTS at higher temperatures. Ca contents are similar at any given temperature in both low- and high-P–high-H_2O runs, but relatively enriched in the HPx-mb16 compositions in the low-H_2O contents at higher temperatures.

Plagioclase anorthite content is systematically higher in HPx-mb16 calculations at any temperature, the difference being greater at higher temperatures.

All calculated orthopyroxene corresponds to enstatite: the compositions are in great agreement between rhyolite-MELTS and HPx-mb16 models and only minor differences can be observed in terms of Si, Al, and X_{Fe3+}.

Amphibole compositions are substantially different between rhyolite-MELTS and HPx-mb16 models as the Green *et al.* (2016) amphibole a–X relations are more complex than the one used in rhyolite-MELTS (Tables S1 and S4). rhyolite-MELTS predicts actinolite and HPx-mb16 predicts pargasite; for instance, Si content in rhyolite-MELTS is 8 atoms per formula unit (a.p.f.u.) whereas the Si predicted in HPx-mb16 is ~6 a.p.f.u. (Table S4). Furthermore, Mg# and Ca contents are systematically higher in rhyolite-MELTS than HPx-mb16 and follow the opposite trend as temperature decreases (Supplementary Table S4).

Garnet compositions are similar between rhyolite-MELTS and the HPx-mb16 models in that all are almandine-rich. However, garnet Mg# are higher in rhyolite-MELTS compared to HPx-mb16 at any given temperature; almandine and grossular contents are systematically higher and pyrope content lower in HPx-mb16 .

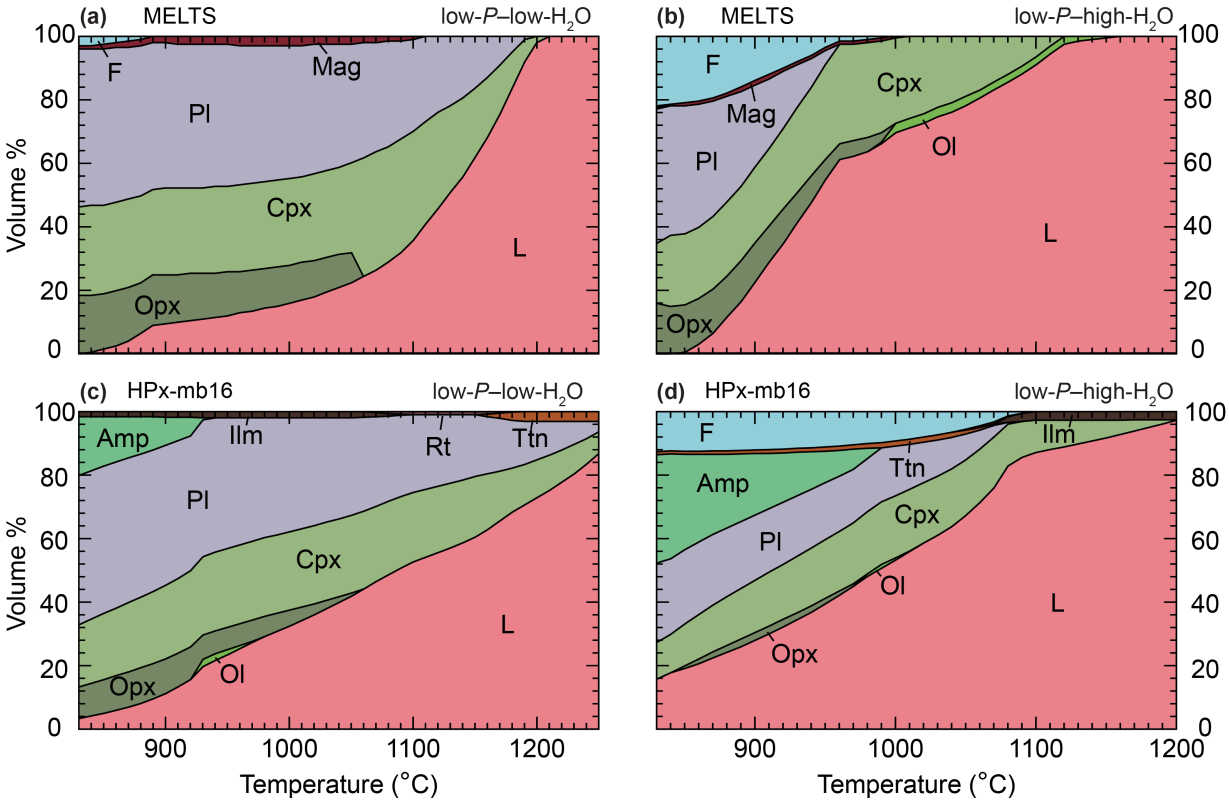

Figure S1. Equilibrium phase assemblages at 0.25 GPa for a N-MORB composition in vol%. (a, b) rhyolite-MELTS and (c, d) HPx-mb16. (a, c) Low-H2O (0.5 wt% H2O) calculations. (b, d) High-H2O (4 wt% H2O) calculations. Mineral abbreviations follow Whitney and Evans (2010) with the exception of "L" and "F" which refer to liquid and fluid, respectively.

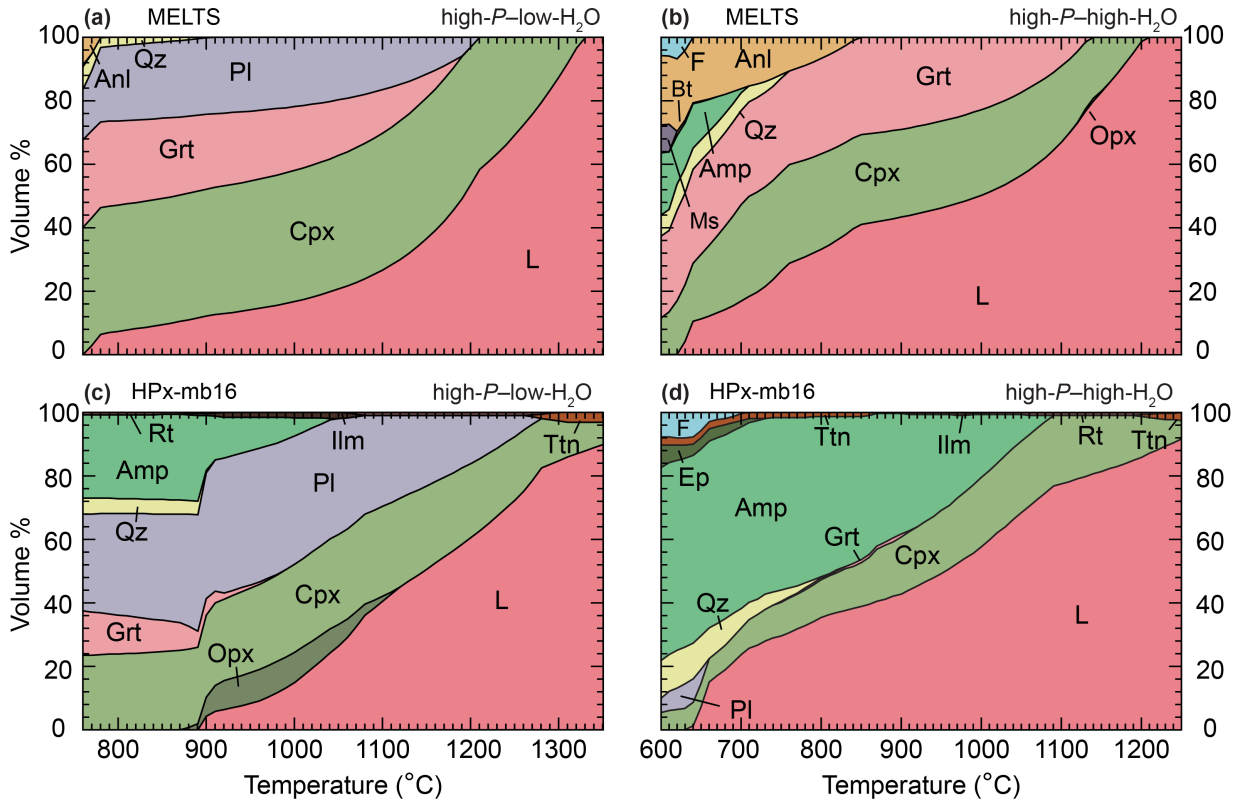

Figure S2. Equilibrium phase assemblages at 1 GPa for a N-MORB composition in vol%. (a, b) rhyolite-MELTS and (c, d) HPx-mb16. (a, c) Low-H_2O (0.5 wt% H_2O) calculations. (b, d) High-H_2O (4 wt% H_2O) calculations. Mineral abbreviations follow Whitney and Evans (2010) with the exception of "L" and "F" which refer to liquid and fluid, respectively.

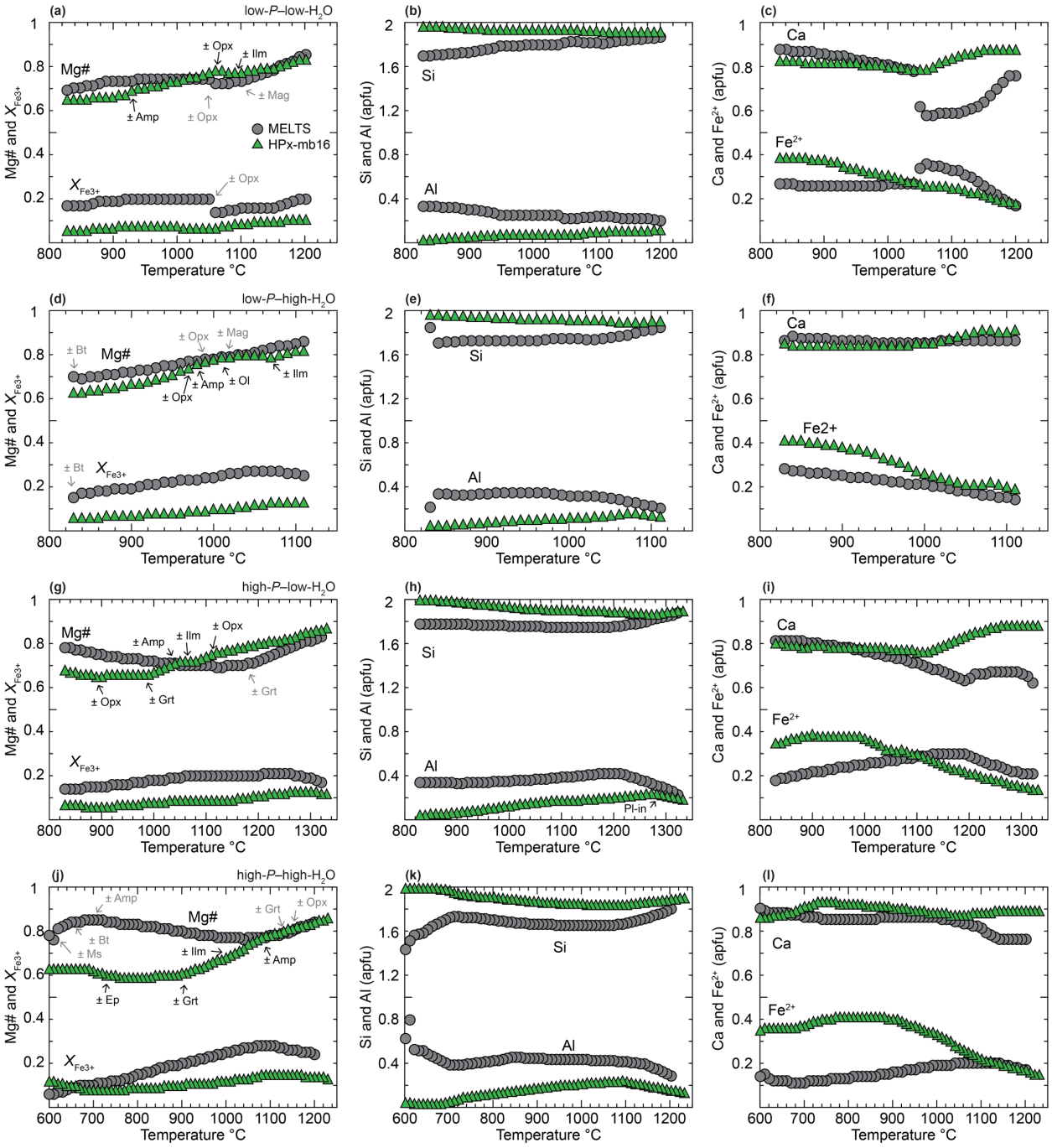

Figure S3. Calculated clinopyroxene compositions (in atoms per formula unit, a.p.f.u.) at (a–f) 0.25 GPa and (g–l) 1 GPa. (a–c and g–i) Clinopyroxene compositions in a low-H_2O (0.5 wt%) MORB composition. (d–f and j–l) Clinopyroxene compositions in a high-H_2O (4 wt%)MORB composition. Mineral abbreviations are the same as in Figure 1.

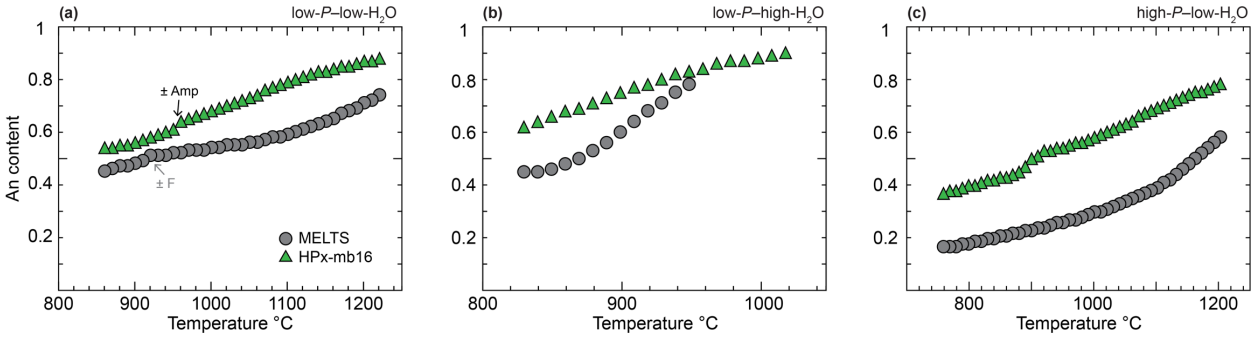

Figure S4. Calculated anorthite content (An) in plagioclase. (a) Plagioclase compositions at 0.25 GPa for a low-H_2O (0.5 wt%) MORB composition. (b) Plagioclase compositions at 0.25 GPa for a high-H_2O (4 wt%) MORB composition. (c) Plagioclase compositions at 1 GPa for a low-H_2O (0.5 wt%) MORB composition. Mineral abbreviations are the same as in Figure 1.

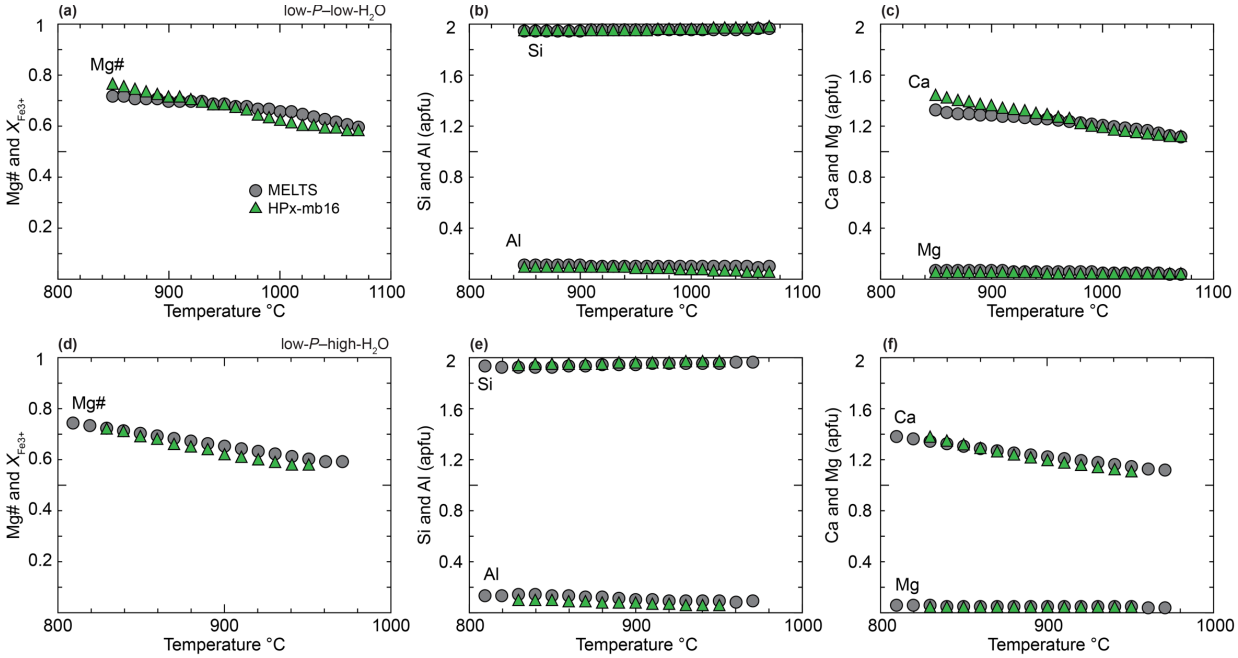

Figure S5. Calculated orthopyroxene compositions (in atoms per formula unit, a.p.f.u.) at 0.25 GPa for a low-H_2O (0.5 wt%) MORB composition.

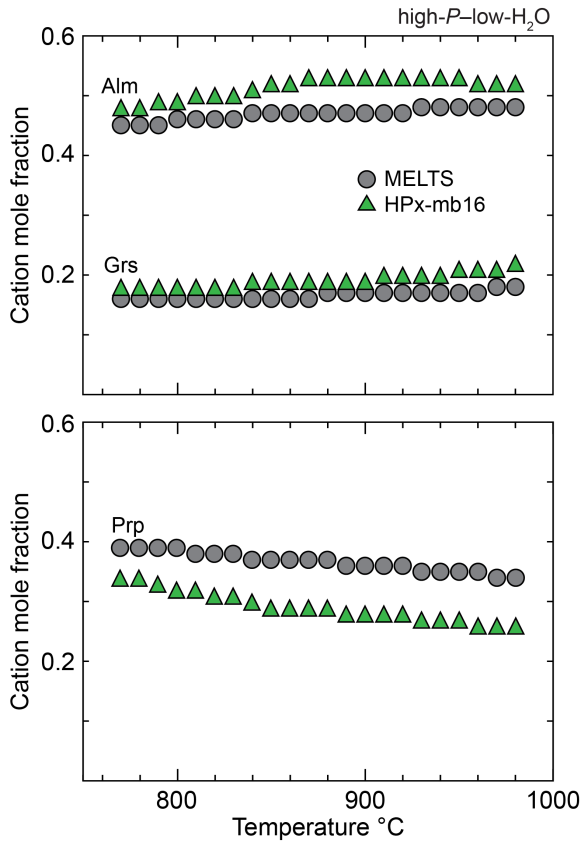

Figure S6. Calculated garnet compositional evolution (in end-member proportions) at 1 GPa for a low-H_2O (0.5 wt%) MORB composition.

Table S1. Components considered in the activity–composition relations used in this work (see text for details).

	Liquid		Olivine		Orthopyroxene		Clinopyroxene		Garnet		Feldspar		Amphibole		Epidtoe	Biotite		Muscovite		Analcime	Ilmenite-Hematite		Spinel-Magnetite	
	MELTS	HPx-mb16	MELTS	HPx-mb16	c	HPx-mb16	MELTS	HPx-mb16	MELTS	HPx-mb16	MELTS	HPx-mb16	MELTS	HPx-mb16	HPx-mb16	MELTS	HPx-mb16	MELTS	HPx-mb16	MELTS	MELTS	HPx-mb16	MELTS	HPx-mb16
SiO_2	x	x	x	x	x	x	x	x	x	x	x	x	x	x	x	x	x	x	x	x				
TiO_2	x				x		x							x			x				x	x	x	x
Al_2O_3	x	x				x	x	x	x	x	x	x	x	x	x	x	x	x	x	x	x		x	x
Cr_2O_3[1]	x																						x	
Fe_2O_3	x				x	x	x	x		x				x	x		x		x		x	x	x	x
FeO	x	x	x	x	x	x	x	x	x	x			x	x	x	x	x		x		x	x	x	x
MnO[1]	x									x							x				x			
MgO	x	x	x	x	x	x	x	x	x	x			x	x		x	x		x		x		x	x
CaO	x	x	x		x	x	x	x	x	x	x	x	x	x	x				x					
Na_2O	x	x			x		x	x			x	x	x	x					x	x				
K_2O	x	x									x	x		x		x	x	x	x	x				
H_2O	x	x											x			x	x	x	x					
P_2O_5[1]	x																							
NiO[1]	x		x																					
CO_2[1]	x																							

[1]Not considered in this work. HPx-mb16–metabasite set (see text for details).

Table S2. Liquid compositions of N-MORB at 0.25 GPa (wt%).

	0.5 wt% H_2O									4 wt% H_2O								
	900 °C			1000 °C			1100 °C			900 °C			1000 °C			1100 °C		
	MELTS	HPx-mb16	% diff.[1]	MELTS	HPx-mb16	% diff.[1]	MELTS	HPx-mb16	% diff.[1]	MELTS	HPx-mb16	% diff.[1]	MELTS	HPx-mb16	% diff.[1]	MELTS	HPx-mb16	% diff.[1]
L fraction (wt.%)	7	9		13	30		32	50		19	26		61	52		88	84	
SiO_2	64.56	58.04	*-10*	61.81	54.41	*-12*	53.61	52.89	*-1*	57.75	59.74	*3*	51.57	52.71	*2*	49.12	49.28	*0*
TiO_2	0.25	–	–	0.73	–	–	1.98	–	–	0.23	–	–	0.64	–	–	1.52	–	–
Al_2O_3	11.74	14.19	*21*	13.53	13.08	*-3*	14.72	13.50	*-8*	17.82	14.63	*-18*	19.88	15.48	*-22*	16.10	17.01	*6*
FeO^t	3.31	10.68	*223*	5.97	15.04	*152*	11.83	15.53	*31*	4.56	7.68	*68*	7.96	10.98	*38*	9.49	10.44	*10*
MgO	1.30	4.00	*208*	2.06	7.05	*242*	3.93	7.76	*97*	0.87	2.76	*219*	2.55	6.11	*140*	5.49	6.64	*21*
CaO	3.89	1.88	*-52*	4.94	2.64	*-47*	6.92	4.43	*-36*	3.17	2.89	*-9*	6.08	4.80	*-21*	10.35	8.43	*-19*
Na_2O	6.13	6.56	*7*	6.03	5.65	*-6*	4.86	4.63	*-5*	6.98	5.99	*-14*	4.39	4.77	*9*	3.09	3.27	*6*
K_2O	1.51	1.09	*-28*	0.90	0.44	*-51*	0.40	0.27	*-32*	0.63	0.48	*-23*	0.22	0.26	*15*	0.15	0.16	*6*
H_2O	7.24	3.56	*-51*	3.91	1.69	*-57*	1.54	1.00	*-35*	7.89	5.82	*-26*	6.57	4.88	*-26*	4.52	4.77	*5*
Total	100	100		100	100		100	100		100	100		100	100		100	100	

[1]difference bewteen HPx-mb16 and MELTS.

Table S3. Liquid compositions of N-MORB at 1 GPa (wt%).

	0.5 wt% H_2O									4 wt% H2O												
	900 °C			1000 °C			1100 °C			800 °C			900 °C			1000 °C			1100 °C		
	MELTS	HPx-mb16	% diff.[1]	MELTS	HPx-mb16	% diff.[1]	MELTS	HPx-mb16	% diff.[1]	MELTS	HPx-mb16	% diff.[1]	MELTS	HPx-mb16	% diff.[1]	MELTS	HPx-mb16	% diff.[1]	MELTS	HPx-mb16	% diff.[1]
L fraction (wt%)	9	3		13	13		22	39		23	27		31	34		38	50		59	73	
SiO_2	74.23	65.72	*-11*	69.67	56.03	*-20*	62.60	51.99	*-17*	66.88	65.45	*-2*	63.72	60.56	*-5*	59.45	53.72	*-10*	52.46	49.39	*-6*
TiO_2	0.51	–	–	0.96	–	–	1.66	–	–	0.06	–	–	0.12	–	–	0.32	–	–	0.89	–	–
Al_2O_3	9.52	14.75	*55*	12.41	14.79	*19*	16.08	14.35	*-11*	6.79	14.63	*115*	9.67	16.88	*75*	12.32	18.10	*47*	15.48	18.25	*18*
FeO^t	0.87	3.84	*339*	2.25	12.90	*474*	5.08	16.82	*231*	0.33	0.55	*67*	1.11	2.90	*162*	3.56	8.15	*129*	8.32	10.55	*27*
MgO	0.48	0.93	*94*	0.78	3.92	*403*	1.33	6.56	*394*	0.42	0.12	*-71*	0.76	0.70	*-9*	1.65	2.58	*57*	3.83	5.18	*35*
CaO	2.23	2.68	*20*	2.98	2.96	*-1*	4.18	4.02	*-4*	2.54	3.30	*30*	3.59	4.58	*28*	5.36	5.95	*11*	7.41	7.21	*-3*
Na_2O	5.36	5.01	*-7*	6.15	5.64	*-8*	6.13	4.64	*-24*	6.59	4.72	*-28*	7.67	4.65	*-39*	6.52	4.10	*-37*	4.42	3.73	*-16*
K_2O	1.19	1.56	*31*	0.90	0.70	*-22*	0.59	0.33	*-44*	0.59	0.41	*-31*	0.44	0.34	*-22*	0.35	0.25	*-29*	0.23	0.19	*-19*
H_2O	5.59	5.51	*-2*	3.86	3.05	*-21*	2.27	1.29	*-43*	15.79	10.81	*-32*	12.89	9.38	*-27*	10.41	7.14	*-31*	6.82	5.51	*-19*
Total	100	100		100	100		100	100		100	100		100	100		100	100		100	100	

[1]difference bewteen HPx-mb16 and MELTS.

Table S4. Amphibole compositions comparison at 1 GPa (wt%).

	600 °C		620 °C		640 °C		660 °C		680 °C		700 °C	
	MELTS	HPx-mb16	MELTS	HPx-mb16	MELTS	HPx-mb16	MELTS	HPx-mb16	MELTS	HPx-mb16	MELTS	HPx-mb16
SiO_2	57.84	42.29	57.9	41.7	58	41.23	58.02	40.89	58.04	40.68	58.05	40.54
TiO_2	–	0.44	–	0.5	–	0.57	–	0.64	–	0.71	–	0.79
Al_2O_3	–	17.17	–	17.57	–	17.88	–	18.09	–	18.12	–	18.12
Fe_2O_3	–	1.3	–	1.29	–	1.27	–	1.25	–	1.24	–	1.22
FeO	5.28	12.73	5.08	12.83	4.75	12.89	4.72	12.9	4.72	12.99	4.74	13.05
MgO	21.49	10.29	21.66	10.2	21.92	10.15	22	10.16	22.08	10.18	22.16	10.22
CaO	13.22	10.36	13.18	10.63	13.15	10.87	13.08	11.08	12.98	11.29	12.87	11.44
Na_2O	–	3.22	–	3.11	–	3.01	–	2.94	–	2.77	–	2.62
K_2O	–	0.2	–	0.18	–	0.16	–	0.08	–	0.07	–	0.06
Total	97.83	98.01	97.83	98.02	97.83	98.03	97.83	98.04	97.83	98.05	97.82	98.06
Oxygens	23	23	23	23	23	23	23	23	23	23	23	23
Si	8.00	6.18	8.00	6.10	8.00	6.04	8.00	6.00	8.00	5.97	8.00	5.95
Ti	–	0.05	–	0.06	–	0.06	–	0.07	–	0.08	–	0.09
Al	–	2.96	–	3.03	–	3.09	–	3.13	–	3.13	–	3.14
Fe^{3+}	–	0.14	–	0.14	–	0.14	–	0.14	–	0.14	–	0.13
Fe^{2+}	0.61	1.56	0.59	1.57	0.55	1.58	0.55	1.58	0.55	1.60	0.55	1.60
Mg	4.43	2.24	4.46	2.23	4.51	2.22	4.52	2.22	4.54	2.23	4.55	2.24
Ca	1.96	1.62	1.95	1.67	1.94	1.71	1.93	1.74	1.92	1.78	1.90	1.80
Na	–	0.91	–	0.88	–	0.86	–	0.84	–	0.79	–	0.75
K	–	0.04	–	0.03	–	0.03	–	0.01	–	0.01	–	0.01
Mg#	0.88	0.59	0.88	0.59	0.89	0.58	0.89	0.58	0.89	0.58	0.89	0.58

Table S5. Phase proportions used for trace-element modeling (wt%).

	low-*P*– low-H_2O at 900 °C		**high-*P*– low-H_2O at 1000 °C**		**high-*P*– high-H_2O at 850 °C**	
	MELTS	HPx-mb16	MELTS	HPx-mb16	MELTS	HPx-mb16
L	7	9	13	13	29	30
Pl	41	40	18	36	–	–
Amp	–	9	–	6	–	51
Opx	18	13	–	11	–	–
Cpx	31	26	44	31	32	16
Ilm	–	3	–	3	–	–
Grt	–	–	25	–	39	1
Ttn	–	–	–	–	–	1
Mag	4	–	–	–	–	–
Total	100	100	100	100	100	100

Mineral abbreviations follow Whitney & Evans (2010) with the exception of “L” which refers to liquid.

Table S6. Partition coefficients from Bédard (2006)

	Cpx	Opx	Pl	Amp	Grt	Mag	Ilm	Ttn
Cs	0.003	0.047	0.087	0.166	0.000	0.001	0.025	0.300
Rb	0.010	0.047	0.068	0.055	0.001	0.001	0.025	0.500
Ba	0.006	0.047	1.016	0.046	0.000	0.001	0.018	1.500
Th	0.104	0.130	0.095	0.055	0.008	0.020	0.090	0.160
U	0.032	0.089	0.091	0.050	0.024	0.020	0.090	0.140
Nb	0.007	0.010	0.239	0.274	0.040	0.040	3.000	2.200
Ta	0.028	0.126	0.053	0.477	0.080	0.040	2.700	6.550
La	0.028	0.000	0.358	0.319	0.028	0.015	0.015	4.730
Ce	0.059	0.001	0.339	0.560	0.080	0.016	0.012	7.570
Pr	0.116	0.001	0.316	0.898	0.150	0.018	0.011	9.000
Pb	0.022	0.047	0.770	0.175	0.032	0.022	0.008	0.040
Sr	0.032	0.047	6.650	0.389	0.019	0.022	0.002	2.680
Nd	0.115	0.003	0.289	1.320	0.222	0.026	0.010	12.400
Sm	0.259	0.009	0.237	2.090	1.430	0.024	0.009	14.000
Zr	0.125	0.031	0.078	0.417	0.537	0.120	2.300	1.920
Hf	0.208	0.246	0.069	0.781	0.431	0.970	2.400	2.430
Ti	0.473	0.500	0.078	4.030	2.630	5.000	12.500	67.000
Eu	0.341	0.680	2.170	1.790	1.540	0.025	0.010	13.800
Gd	0.422	0.020	0.192	2.530	4.840	0.018	0.011	11.900
Tb	0.502	0.030	0.170	2.600	7.800	0.019	0.018	10.000
Dy	0.570	0.043	0.150	2.550	11.500	0.018	0.020	8.270
Y	0.603	0.054	0.138	2.470	14.100	0.018	0.037	5.420
Ho	0.616	0.060	0.132	2.410	15.300	0.018	0.035	5.500
Er	0.640	0.079	0.117	2.220	18.800	0.018	0.067	5.540
Tm	0.644	0.101	0.104	2.000	21.500	0.018	0.102	4.000
Yb	0.635	0.125	0.094	1.790	23.200	0.018	0.130	3.020
Lu	0.617	0.149	0.085	1.590	24.100	0.018	0.190	2.000

Mineral abbreviations follow Whitney & Evans (2010).